

# SCIENTIFIC REPORTS

OPEN

## AIM2 Inflammasome-Mediated Pyroptosis in Enterovirus A71-Infected Neuronal Cells Restricts Viral Replication

Thinesswary Yogarajah<sup>1</sup>, Kien Chai Ong<sup>2</sup>, David Perera<sup>3</sup> & Kum Thong Wong<sup>1</sup>

Encephalomyelitis is a well-known complication of hand, foot, and mouth disease (HFMD) due to Enterovirus 71 (EV71) infection. Viral RNA/antigens could be detected in the central nervous system (CNS) neurons in fatal encephalomyelitis but the mechanisms of neuronal cell death is not clearly understood. We investigated the role of absent in melanoma 2 (AIM2) inflammasome in neuronal cell death, and its relationship to viral replication. Our transcriptomic analysis, RT-qPCR, Western blot, immunofluorescence and flow cytometry studies consistently showed AIM2 gene up-regulation and protein expression in EV-A71-infected SK-N-SH cells. Downstream AIM2-induced genes, CARD16, caspase-1 and IL-1 $\beta$  were also up-regulated and caspase-1 was activated to form cleaved caspase-1 p20 subunits. As evidenced by 7-AAD positivity, pyroptosis was confirmed in infected cells. Overall, these findings have a strong correlation with decreases in viral titers, copy numbers and proteins, and reduced proportions of infected cells. AIM2 and viral antigens were detected by immunohistochemistry in infected neurons in inflamed areas of the CNS in EV-A71 encephalomyelitis. In infected AIM2-knockdown cells, AIM2 and related downstream gene expressions, and pyroptosis were suppressed, resulting in significantly increased virus infection. These results support the notion that AIM2 inflammasome-mediated pyroptosis is an important mechanism of neuronal cell death and it could play an important role in limiting EV-A71 replication.

Enterovirus A71 (EV-A71) is a human RNA virus that belongs to the species A group, *Enterovirus* genus and *Picornaviridae* family. The virion is about 30 nm and contains a single-stranded, positive-sense RNA genome of approximately 7.5 kb. EV-A71 causes sporadic and epidemic hand, foot and mouth disease (HFMD), a common infectious disease most frequently seen in young children aged 5 and below<sup>1-3</sup>. Since its initial isolation and identification in 1969<sup>4</sup>, numerous large outbreaks of HFMD have been reported worldwide<sup>5-13</sup>. EV-A71-associated HFMD is occasionally associated with central nervous system (CNS) complications, such as aseptic meningitis, acute flaccid paralysis and encephalomyelitis<sup>14-19</sup>. Based on autopsy findings in fatal cases of EV-A71 encephalomyelitis, it is clear that CNS neurons are the main viral targets since neuronal degeneration/necrosis and neuronophagia were readily observed. Moreover, viral antigens and RNA localized almost exclusively to these cells<sup>20,21</sup>. Thus, viral-induced cell death or viral cytolysis in neurons plays a major role in neuropathogenesis<sup>22,23</sup>.

Classically, neuronal cell death may result from apoptosis and necrosis<sup>24</sup>. Nonetheless, recent advances in understanding of cell death mechanisms suggest that apart from apoptosis, other complex mechanisms such as pyroptosis, autophagy and necroptosis may be involved in viral infection<sup>25-28</sup>. Even though both pyroptosis and necroptosis are programmed cell death mechanisms and promote inflammation, these pathways differ in their initiators; pyroptosis is induced via inflammasomes and caspase-1 activation, while necroptosis involves receptor-interacting protein kinase 3<sup>29</sup>. Moreover, both mechanisms are distinct from autophagy that causes activation of microtubule-associated protein 1A/1B-light chain 3 and formation of autophagosomes. Studies have shown that EV-A71 infection can cause apoptosis in cell lines such as rhabdomyosarcoma, human neuroblastoma (SK-N-SH, SK-N-MC and SH-SY5Y) and human glioblastoma cells<sup>30-34</sup>. Specifically, protein expression

<sup>1</sup>Department of Pathology, Faculty of Medicine, University of Malaya, Kuala Lumpur, Malaysia. <sup>2</sup>Department of Biomedical Science, Faculty of Medicine, University of Malaya, Kuala Lumpur, Malaysia. <sup>3</sup>Institute of Health and Community Medicine, University Malaysia Sarawak, Sarawak, Malaysia. Correspondence and requests for materials should be addressed to K.T.W. (email: [wongkt@ummc.edu.my](mailto:wongkt@ummc.edu.my))

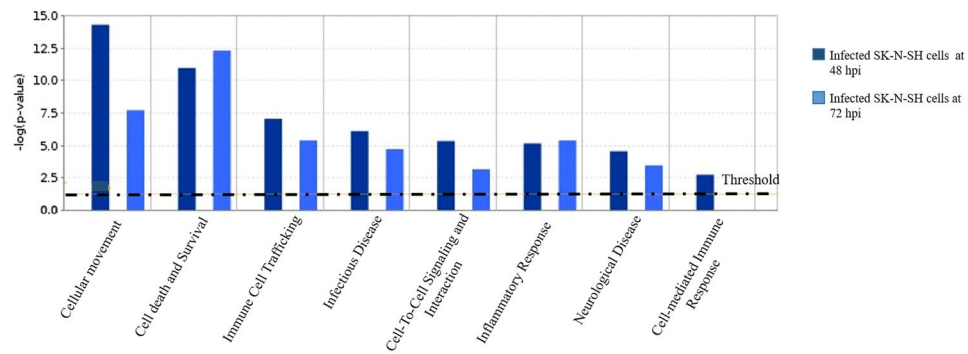


**Figure 1.** Disease and function pathways derived from transcriptome and Ingenuity pathway analysis of infected SK-N-SH cells. The most highly up-regulated disease and function genes involved cellular movement and cell death/survival. The graph shows the category scores where the “threshold” indicates the minimum significance level [calculated as  $-\log(p\text{-value})$  using the Fisher’s exact test, set at 1.25].

of cleaved caspase-9 was shown in EV-A71-infected SK-N-SH cells indicating cells undergo apoptosis. On the other hand, in our previous study, we have been unable to demonstrate apoptosis in SK-N-SH cells; the evidence had suggested neuronal necrosis<sup>35</sup>. Moreover, apoptosis has also not been convincingly demonstrated in infected CNS neurons in fatal human EV-A71 encephalomyelitis, although neuronal necrosis by viral cytolysis were well documented<sup>20,36–38</sup>.

We investigated the specific mechanisms, which may be involved in neuronal death induced by EV-A71 as this phenomenon remains under-investigated. In particular, we examined the role of pyroptosis, a recently described novel programmed cell death mechanism which is characterized by caspase 1 activation, DNA breakages without laddering, cell swelling, plasma membrane rupture and release of intracellular contents of pro-inflammatory cytokines<sup>39,40</sup>. Pyroptosis was first characterized in *Salmonella*<sup>41</sup> and *Shigella*<sup>42</sup> infections and recently also described in adenovirus, encephalomyocarditis virus and rhinovirus infections in non-neuronal human cell lines<sup>43–45</sup>. As far as we are aware, pyroptosis in neurons has only been described in acute brain injuries such as stroke and trauma, and neurodegenerative diseases such as Alzheimer’s and Parkinson’s diseases<sup>46–48</sup>.

During pyroptosis, caspase-1 forms part of, and is activated by, a large supramolecular complex known as inflammasome that may also comprise other proteins such as “PYD and CARD Containing Domain” (PYCARD). Inflammasome assembly may be initiated by various protein activators including “absent in melanoma 2” (AIM2), “NOD-like-Receptor Protein” (NLRP) or “RNA Sensor Retinoic Acid-inducible Gene-1” (RIG-I)<sup>49–51</sup>. AIM2-activated inflammasome or AIM2 inflammasome is known to be generally triggered by cytosolic DNA from both bacteria (*Listeria monocytogenes*)<sup>52</sup> and viral (murine cytomegalovirus<sup>53</sup> and vaccinia virus)<sup>54,55</sup>. RNA viruses that trigger AIM2 inflammasome includes Chikungunya virus and West Nile Virus (WNV)<sup>56</sup>. Other RNA viruses trigger NLRP inflammasome assembly (influenza, dengue virus and hepatitis C)<sup>57</sup>, and RIG-I inflammasome (vesicular stomatitis virus and encephalomyocarditis virus)<sup>57</sup>. Once formed these inflammasomes lead to caspase-1 activation, a process promoted by Caspase Recruitment Domain Family Member 16 (CARD16)<sup>58,59</sup>. Pro-caspase-1 is cleaved to its activated form, caspase-1 p20 subunits, which in turn activates inflammatory cytokines, Interleukin (IL)-18 and IL-1 $\beta$  in addition to inducing pyroptosis<sup>46,60</sup>.

To date, there is no evidence of AIM2 inflammasome formation and pyroptosis in EV-A71 infection. In this study, we first performed microarray/transcriptome analysis on human neuroblastoma (SK-N-SH) cells following EV-A71 infection. Based on findings that suggested involvement of AIM2 inflammasome, we hypothesized that pyroptosis may be an important mechanism in EV-A71-induced neuronal cell death. We further performed RT-qPCR analysis, western blotting, immunofluorescence and flow cytometry in infected cells, and immunohistochemistry on human autopsy tissues of EV-A71 encephalomyelitis to confirm this. We found that AIM2 and caspase-1 upregulation reduces EV-A71 replication by inducing pyroptosis in SK-N-SH cells. AIM2 expression in human CNS tissues of EV-A71 encephalomyelitis was also demonstrated. Our results highlight the importance of AIM2 inflammasome and pyroptosis in EV-A71 neuronal infection.

## Results

**Transcriptome analysis of EV-A71 infection in SK-N-SH cells.** We analyzed the effect of EV-A71/13903 infection in human SK-N-SH cells at the gene expression level when >50% infection was achieved (Supplementary Figure S1). Among 24,000 genes analyzed, pairwise comparisons between infected and uninfected cells at  $\geq 2$ -fold change threshold, showed 287 up-regulated genes and 390 down-regulated genes at 48 hpi, and 702 up-regulated and 674 down-regulated genes at 72 hpi (Gene expression omnibus accession: GSE71673). These genes were classified according to their molecular and cellular functions using the Ingenuity pathway analysis software, which showed that the most dysregulated genes involved cellular movement, and cell death and survival (Fig. 1). Among the most highly up-regulated genes, only AIM2 is associated with cell death/survival, while other genes were associated with cellular movement, cell death/survival or other functions (Table 1). Up-regulation of downstream of AIM2-mediated, pyroptosis-associated genes, CARD16 and caspase-1 was also observed (Table 1). However, IL-1 $\beta$  showed a 1.98 fold change while IL-18 expression was not

48 hpi			72 hpi		
Fold Change	ANOVA p-value	Gene	Fold Change	ANOVA p-value	Gene
<b>Topmost-upregulated genes ranked by degree of fold change</b>					
13.35	0.044962	Chemokine (C-X-C motif) ligand 11 (CXCL11)	15.26	0.003415	Serine peptidase inhibitor, Kazal type 6
9.3	0.039725	Cathepsin S	14.13	0.016601	Chemokine (C-C motif) ligand 5
9.17	0.000695	superoxide dismutase 2, mitochondrial (CSF2)	13.73	0.000022	Deleted in lymphocytic leukemia 2 (non-protein coding)
<b>7.92</b>	<b>0.000113</b>	<b>Absent in melanoma 2 (AIM2)</b>	9.96	0.000025	Colony stimulating factor 2 (granulocyte-macrophage)
7.4	0.005032	Tumor necrosis factor, alpha-induced protein 6 (TNFAIP6)	8.99	0.015315	Chemokine (C-X-C motif) ligand 11
7.31	0.036801	Interleukin 8 (IL-8)	7.2	0.000796	Tumor necrosis factor, alpha-induced protein 6
6.95	0.026789	Zinc finger CCCH-type, antiviral 1	7.17	0.000134	Family with sequence similarity 111, member B (FAM111B)
6.56	0.01899	Chemokine (C-C motif) ligand 20 (CCL20)	6.86	0.000719	Cathepsin S
6.47	0.040204	Chemokine (C-C motif) ligand 5 (CCL5)	6.67	0.000206	superoxide dismutase 2, mitochondrial
5.57	0.00589	Laminin, beta 3	6.64	0.006316	Chemokine (C-C motif) ligand 5
5.39	0.030611	Colony stimulating factor 2 (granulocyte-macrophage) (CSF2)	6.29	0.000198	Family with sequence similarity 111, member B
5.08	0.002999	Interleukin 6 (interferon, beta 2) (IL-6)	6.25	0.000991	Interleukin 8
5	0.01762	Interferon-induced protein with tetratricopeptide repeats 2	<b>6.19</b>	<b>0.00103</b>	<b>Absent in melanoma 2 (AIM2)</b>
4.91	0.039786	SP100 nuclear antigen	5.96	0.009354	Chemokine (C-C motif) ligand 20
4.89	0.015657	Tumor necrosis factor, alpha-induced protein 3 (TNFAIP3)	5.7	0.000114	Chemokine (C-X-C motif) ligand 3
4.84	0.025299	Cathepsin S	5.59	0.001701	Cell division cycle 25 A
4.37	0.012194	Serine peptidase inhibitor, Kazal type 6	5.58	0.01762	Chemokine (C-X-C motif) ligand 10 (CXCL10)
4.31	0.042266	Chemokine (C-X-C motif) ligand 3 (CXCL3)	5.28	0.003336	Chemokine (C-X-C motif) ligand 1
<b>AIM2-mediated, pyroptosis-associated genes</b>					
3.02	0.030757	Caspase 1 (CASP1)	2.16	0.009802	Caspase recruitment domain family, member 16 (CARD16)
2.12	0.031591	Caspase recruitment domain family, member 16 (CARD16)	2.01	0.016223	Caspase 1 (CASP1)
ND	ND	Interleukin 1, beta (IL-1 $\beta$ )	1.98	0.672011	Interleukin 1, beta (IL-1 $\beta$ )

**Table 1.** Selected up-regulated genes in EV-A71/13903 infected SK-N-SH cells at 48 and 72 hours post-infection (hpi). The fold change threshold used to determine gene up-regulation was  $\geq 2.00$  relative to mock-infected cells. ANOVA p-values were derived from the two-way ANOVA statistical test:  $p \leq 0.05$  is significant. AIM2 fold change was 7.92 at 48 hpi and 6.19 at 72 hpi (**highlighted in bold**). \*ND = not detectable.

detected. To confirm that AIM2 up-regulation was not restricted to EV-A71/13903, RT-qPCR was performed on EV-A71/18431 and EV-A71/SB12736 infected SK-N-SH cells, and the results show AIM2 up-regulation as well (Fig. 2).

**RT-qPCR validation of AIM2, CARD16, Caspase-1 and IL-1 $\beta$  up-regulation in infected SK-N-SH cells.** Reconfirmation of AIM2 expression and up-regulation of downstream pyroptosis-associated genes CARD16, caspase-1 and IL-1 $\beta$  was validated using RT-qPCR (Fig. 3). At 48 and 72 hpi, consistent with, but much higher than transcriptome results, AIM2 was up-regulated by 90 and 105 folds, respectively, compared to mock-infected cells (Fig. 3a). At the additional time points of 24 and 96 hpi, the AIM2 fold change was 320 and 80, respectively. Overall, AIM2 fold change was maximum at 24 hpi. From 48 to 96 hpi, AIM2 expression dropped slightly and plateaued.

Caspase-1 expression was uniformly increased by 4–5 folds for all time points (Fig. 3b). The CARD16 expression was increased at 24, 48 and 72 hpi but not at 96 hpi (Fig. 3d). Thus, RT-qPCR results confirmed our transcriptome analysis showing AIM2, CARD16 and caspase-1 up-regulation in EV-A71/13903-infected SK-N-SH cells. Furthermore, in contrast to transcriptome results, IL-1 $\beta$  showed a significant 10–15 folds increase for all time points (Fig. 3e).

To determine that EV-A71 viral RNA alone was also able to trigger AIM2 up-regulation, we transfected EV-A71/13903 RNA into SK-N-SH cells. AIM2 gene was highly expressed (21 fold) at 12 and 24 hpi (22 fold)

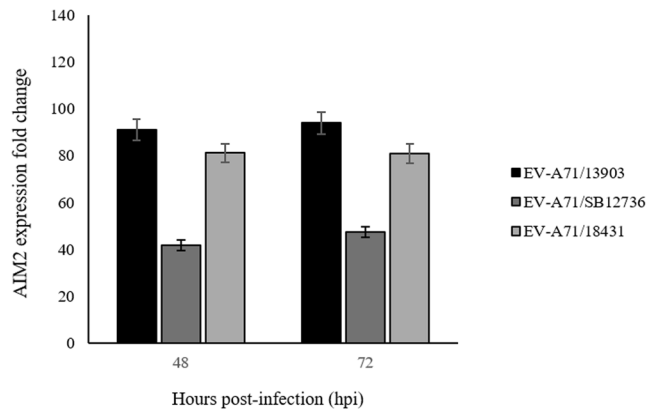


**Figure 2.** EV-A71 strains up-regulated AIM2 expression in infected SK-N-SH cells. AIM2 expression in infected SK-N-SH cells determined by real-time PCR analysis in all three EV-A71 strains (13903, 18431, and SB12736) showed significantly higher AIM2 fold change relative to mock-infected controls at 48 and 72 hpi. All data represent the mean  $\pm$  standard deviation of a set of triplicates.

(Fig. 3f), in tandem with elevation of caspase-1 expression at 12 (2 fold) and 24 hpt (3 fold) (Fig. 3g) compared to mock-transfected cells. EV-A71/13903 viral copies were detected from 12 to 24 hpt (Fig. 3h). Transfection of SK-N-SH cells using UV inactivated viral RNA did not up-regulate AIM2 expression at 12 hpt (0.9 folds) and 24 hpt (1.2 folds), and caspase-1 expression at 12 hpt (1.2 folds) and 24 hpt (1.1 folds) (Fig. 3f and g).

**AIM2 knockdown reduced caspase-1, CARD16, IL-1 $\beta$  and increased viral replication.** Infected AIM2 knockdown (SK-N-SH/siAIM2) cells showed a marked decrease (>50%) of AIM2 expression from 24 to 96 hpi with the lowest levels after 24 hpi (Fig. 3a). Western blot analysis confirmed that AIM2 proteins were nearly undetectable at 72 hpi (Fig. 3a). There was significant concomitant decrease of CARD16 ( $p < 0.05$ , Fig. 3d) and caspase-1 ( $p < 0.05$ , Fig. 3b) expression for all time points. By Western blot analysis, cleaved caspase-1 p20 subunits (activated caspase-1) was absent in infected SK-N-SH/siAIM2 cells but pro-caspase-1 (unactivated caspase-1) was present (Fig. 3b). Moreover, significant decrease of IL-1 $\beta$  expression (Fig. 3e) for all time points was observed. The positive (siRNA GAPDH knockdown) and siRNA negative controls showed expected results (Supplementary Figure S2a). The results showed transfection efficiency of siRNA of 86% and 98% as shown in siGLO-expressing SK-N-SH cells at 72 and 96 hpt, respectively, was considered acceptable. 7-AAD positivity was low (ranging from 1 to 8%) at 24 to 144 hpt (Supplementary Figure S2b).

In contrast to SK-N-SH cells, infected SK-N-SH/siAIM2 cells showed significantly higher viral RNA copies (10 fold higher;  $p < 0.05$ ) (Fig. 3c), viral titers ( $\sim 2$  folds overall;  $p < 0.05$ ) for all time points (Fig. 4), and much higher viral antigens at 72 hpi (Fig. 3c) by Western blot analysis. At lower MOIs of 0.1 and 1, viral titers were also significantly higher ( $\sim 2$  folds overall;  $p < 0.05$ ) in SK-N-SH/siAIM2 cells, suggesting that the pattern of viral replication is the same regardless of the size of inoculum (Fig. 4).

Cell swelling suggestive of pyroptosis was observed only in infected SK-N-SH cells from 48 hpi onwards but not in infected SK-N-SH/siAIM2 cells (Fig. 5a). This result correlated with flow cytometry analysis of 7-AAD staining in infected SK-N-SH cells which showed significant increase at 48 hpi (Fig. 5b). Conversely, cell shrinkage and detachment were observed in infected SK-N-SH/siAIM2 cells from 48 hpi (Fig. 5c). Similarly, flow cytometry analysis of infected SK-N-SH/siAIM2 cells showed only about 6% of 7-AAD positivity throughout (Fig. 5d).

Taken together, the data suggest that AIM2 knockdown reduced CARD16, activated caspase-1 and IL-1 $\beta$ , resulting in amelioration of AIM2 inflammasome suppression of EV-A71 replication in SK-N-SH cells.

### Co-localization of viral and AIM2 antigens in infected SK-N-SH and SK-N-SH/siAIM2 cells.

Generally, we were able to demonstrate co-localization of viral antigens and AIM2 protein in most infected cells by double IF at all time points (Fig. 6a–d; arrows) but mock-infected cells showed very little to no AIM2 positivity (data not shown). AIM2 expression was found to be maximum at 72 and 96 hpi in infected SK-N-SH cells. At these late time points, viral antigens were reduced or absent (arrowhead; Fig. 6c,d) compared to 24 and 48 hpi when viral antigens were more evident. In infected SK-N-SH/siAIM2 cells, AIM2 was absent in all cells at all time points. However, viral antigens gradually increased from 24 hpi, and almost all cells were viral antigen-positive by 72 and 96 hpi (Fig. 6a–d; arrows).

Flow cytometry analysis further confirmed that infected SK-N-SH cells and demonstrated significantly lower percentage of viral antigens of about 40% (Fig. 7a,I) at 48 hpi ( $p = 0.0002$ ), and about 46% (Fig. 7c,I) at 96 hpi ( $p = 0.0009$ ) compared to infected SK-N-SH/siAIM2 cells and at about 73% (Fig. 7b,I) and 96% (Fig. 7d,I), respectively. In SK-N-SH cells, although there were fewer viral antigen-positive cells, about 85% and 80% at 48 (Fig. 7a,IV) and 96 hpi (Fig. 7c,IV), respectively, were AIM2 positive. However, in SK-N-SH/siAIM2 cells, despite the higher number of viral antigen-positive cells, AIM2 was positive in only about 6% and 5% of cells at 48 (Fig. 7b,IV) and 96 hpi (Fig. 7d,IV), respectively.

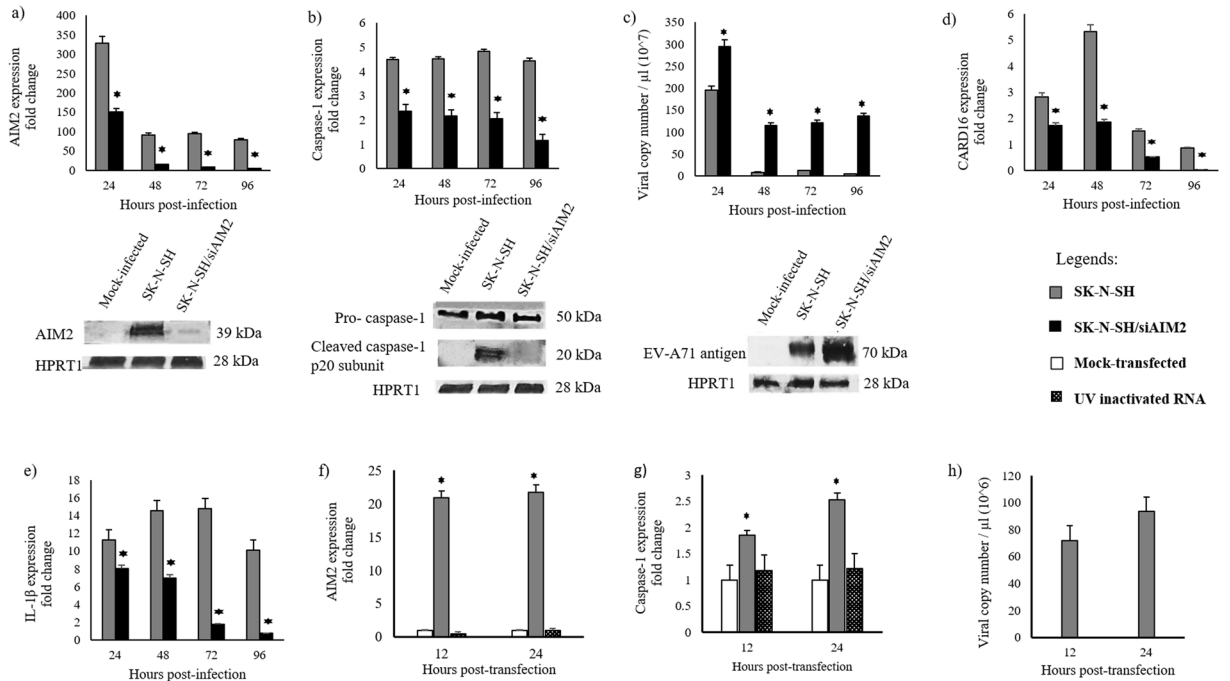


**Figure 3.** AIM2, CARD16, caspase-1 and IL-1 $\beta$  up-regulation, caspase-1 activation and viral replication inhibition was observed in infected-SK-N-SH cells but not in SK-N-SH/siAIM2 cells. There was up-regulation of AIM2 (a), caspase-1 (b), CARD16 (d) and IL-1 $\beta$  (e) expressions in infected SK-N-SH cells, and significant reduction (\* $p < 0.05$ ) in SK-N-SH/siAIM2 cells. Western blot analysis showed a marked reduction/absence of AIM2 protein (a) and cleaved caspase-1 p20 subunits (activated caspase-1). Cropped blots are presented due to different primary and secondary antibody procedures during staining. (b) Viral copy numbers (c) were about 10 fold higher (\* $p < 0.05$ ) in infected SK-N-SH/siAIM2 cells for all time points, corresponding to Western blot analysis that showed much higher viral proteins in infected cells (c). AIM2 (f) and caspase-1 (g) gene expressions in EV-A71/13903 viral RNA transfected SK-N-SH cells showed significant up-regulation (\* $p < 0.05$ ) at 12 and 24 hpt, respectively. UV-inactivated EV-A71/13903 RNA transfection showed no up-regulation of AIM2 (f) and caspase-1 (g) gene expression at both time points. Viral copies at 12 to 24 hpt in viral RNA transfected SK-N-SH cells were detected but the apparent differences were not statistically significant ( $p = 0.7009$ ) (h). All data represent the mean  $\pm$  standard deviation of a set of triplicates.

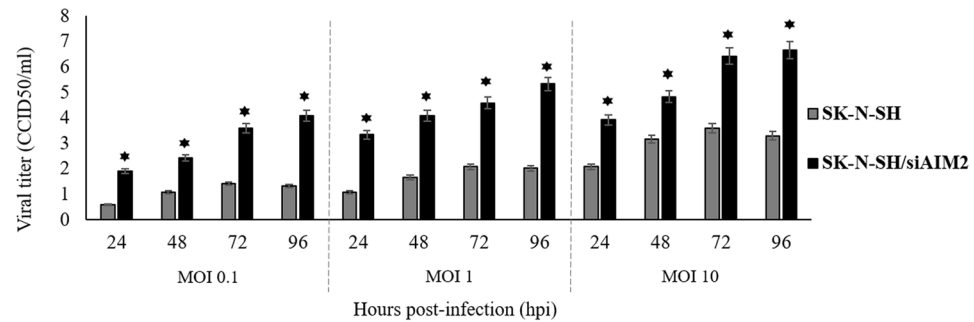


**Figure 4.** Viral replication inhibition did not depend on multiplicity of infection. (a) Viral titration of EV-A71/13903-infected SK-N-SH and SK-N-SH/siAIM2 cells at MOIs of 0.1, 1 and 10. Significantly lower (\* $p < 0.05$ ) viral titers were observed in infected SK-N-SH cells compared to SK-N-SH/siAIM2 for all time points at all MOIs. In SK-N-SH/siAIM2 cells, a gradual increase in viral titers were observed from 24 to 72 hpi, while in SK-N-SH cells no significant increase was observed after 48 hpi. All data represent the mean  $\pm$  standard deviation of a set of triplicates.

**AIM2 correlates with 7-AAD staining in infected SK-N-SH and SK-N-SH/siAIM2 cells.** To determine loss of cell membrane integrity, an inherent feature of pyroptosis, we stained for 7-AAD in infected SK-N-SH cells. Cells triple-stained with 7-AAD, AIM2 and viral antigens were analyzed by flow cytometry to study their correlation. Results showed 7-AAD positivity in about 53% (48 hpi; Fig. 7a,II) and 41% (96 hpi; Fig. 7c,II) in AIM2-positive cells and about 51% (48 hpi; Fig. 7a,III) and 40% (96 hpi; Fig. 7c,III) of viral antigen-positive

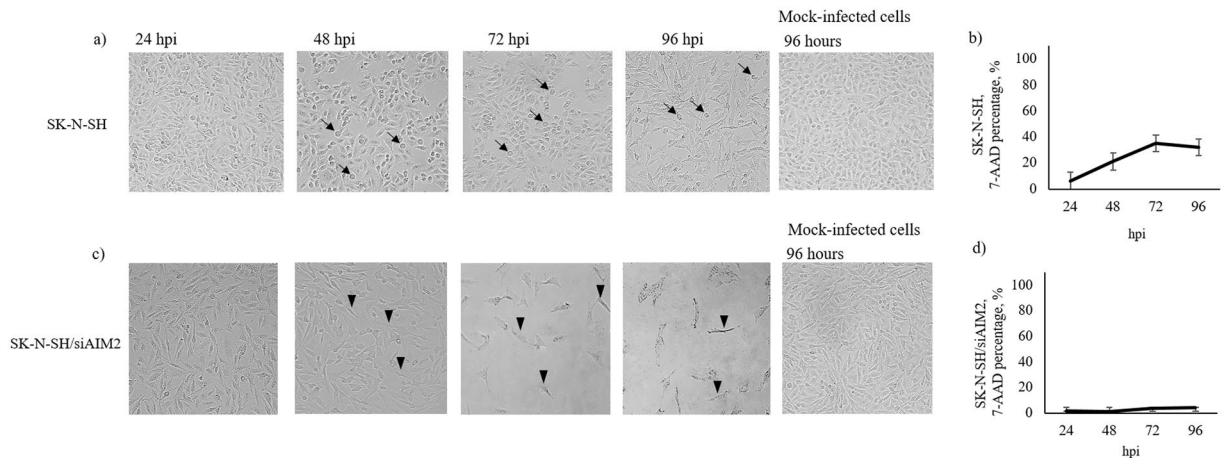


**Figure 5.** Cell swelling correlated with 7-AAD staining in infected SK-N-SH and SK-N-SH/siAIM2 cells. (a) Cellular morphology of EV-A71/13903-infected SK-N-SH cells at MOI of 10 showed pyroptotic cell swelling (arrows) from 48 hpi. (b) Flow cytometry analysis of percentage of the 7-AAD positive infected SK-N-SH cells showed significant increase from at 24 hpi onwards. (c) In contrast, SK-N-SH/siAIM2 cells showed extensive cell shrinkage (arrow heads) and detachment rather than swelling from 48 hpi onwards. (d) This correlated with the percentage of 7-AAD stained infected SK-N-SH/siAIM2 cells was low at about 6% throughout. All data represent the mean  $\pm$  standard deviation of a set of triplicates.

cells. In contrast, infected SK-N-SH/siAIM2 cells showed only about 1% (48 hpi; Fig. 7b,II) ( $p = 0.0002$ ) and 4% (96 hpi; Fig. 7d,II) ( $p = 0.001$ ) 7-AAD positivity in AIM2-positive cells, and about 1% (48 hpi; Fig. 7b,III) ( $p = 0.0001$ ) and 4% (96 hpi; Fig. 7d,III) ( $p = 0.001$ ) of viral antigen-positive cells. AIM2 protein was absent in mock-infected SK-N-SH cells (Supplementary Figure S3) confirming results shown by Western blot (Fig. 3a). Positive staining controls showed expected results (Supplementary Figure S3).

Figure 7e and f show graphs that correlate the percentage of infected cells that were AIM2, 7-AAD and viral antigen positive over various time points. In SK-N-SH cells (Fig. 7e), at 24 hpi, there was a low percentage of AIM2 and 7-AAD positivity (about 5%) while there was a high percentage of viral antigen positive cells (about 45%). However, at 48 hpi, a significant increase in AIM2 and 7-AAD positivity with a decrease in viral antigen positive cells were observed. At 72 and 96 hpi, percentage of AIM2, 7-AAD and viral antigen positive cells plateaued at about 40%. On the other hand, in SK-N-SH/siAIM2 cells (Fig. 7f), very low AIM2 and 7-AAD-positive cells were observed for all time points but there was significant increase in viral antigen-positive cells from 24 to 96 hpi. This suggests that pyroptosis (7-AAD positivity) occurs only in AIM2-expressing infected SK-N-SH cells, and was significantly reduced in SK-N-SH/siAIM2 cells, and that AIM2 induced pyroptosis inhibits viral replication in SK-N-SH cells.

**AIM2 was highly expressed in the CNS tissues of human EV-A71 encephalomyelitis patients.** To confirm the *in vitro* findings, IHC staining was performed to localize AIM2 protein in human CNS tissues of 3 autopsies. The spinal cord, medulla, pons, midbrain and the cerebral cortex were IHC stained with viral antigens or AIM2 protein (Fig. 8). AIM2-positive cells were detected in spinal cords (arrows, Fig. 8a,b) and medullas (arrows; Fig. 8c) only in the inflamed areas in all 3 cases. In one case, EV-A71 viral antigens (arrow; Fig. 8e,g and i) was demonstrated in the same neurons where AIM2 was positive (arrow, Fig. 8f,h and j), while some neurons were AIM2 positive but viral antigen negative (arrowheads, Fig. 8e,f and g,h). In all 3 cases there was no AIM2 staining in the cerebral cortex (Fig. 8d) and other regions where inflammation were absent.

## Discussion

Hitherto, the exact mechanism of neuronal cell death in EV-A71 encephalomyelitis remains unclear. Our study strongly suggests that AIM2 inflammasome-induced pyroptosis following EV-A71 infection is an important cell death mechanism in neurons. AIM2 plays a critical role in the downstream activation of caspase-1 and CARD16 leading to AIM2 inflammasome assembly that triggers pyroptosis and the activation of IL-1 $\beta$  and IL-18<sup>61</sup>. Activated IL-1 $\beta$  amplifies inflammatory response by stimulating immune cell activation<sup>61</sup> while IL-18 stimulates production of IFN- $\gamma$ <sup>62</sup>. Pyroptosis also releases other intra-cytoplasmic pro-inflammatory cytokines<sup>63</sup>.

We used a high throughput transcriptome platform and the Ingenuity pathway analysis to study gene expressions as initial screening of neuronal responses to infection, and found that the most up-regulated genes were involved in cell movement, cell death/survival and immune cell trafficking pathways (Fig. 1). We chose to focus on AIM2 as it is the only highly up-regulated gene involved specifically in pyroptosis, a novel pro-inflammatory cell death mechanism characterized by caspase-1 activation, DNA breakages without laddering, cell swelling, plasma membrane rupture and pro-inflammatory cytokine release<sup>41</sup>. Recent studies have described the importance of inflammasomes in suppressing virus replication<sup>57</sup>, thus a better understanding may provide potential tools for intervention strategies in viral infections. Moreover, in the transcriptome analysis, other highly up-regulated genes were not related to cell death/survival processes such as apoptosis, autophagy or necroptosis.

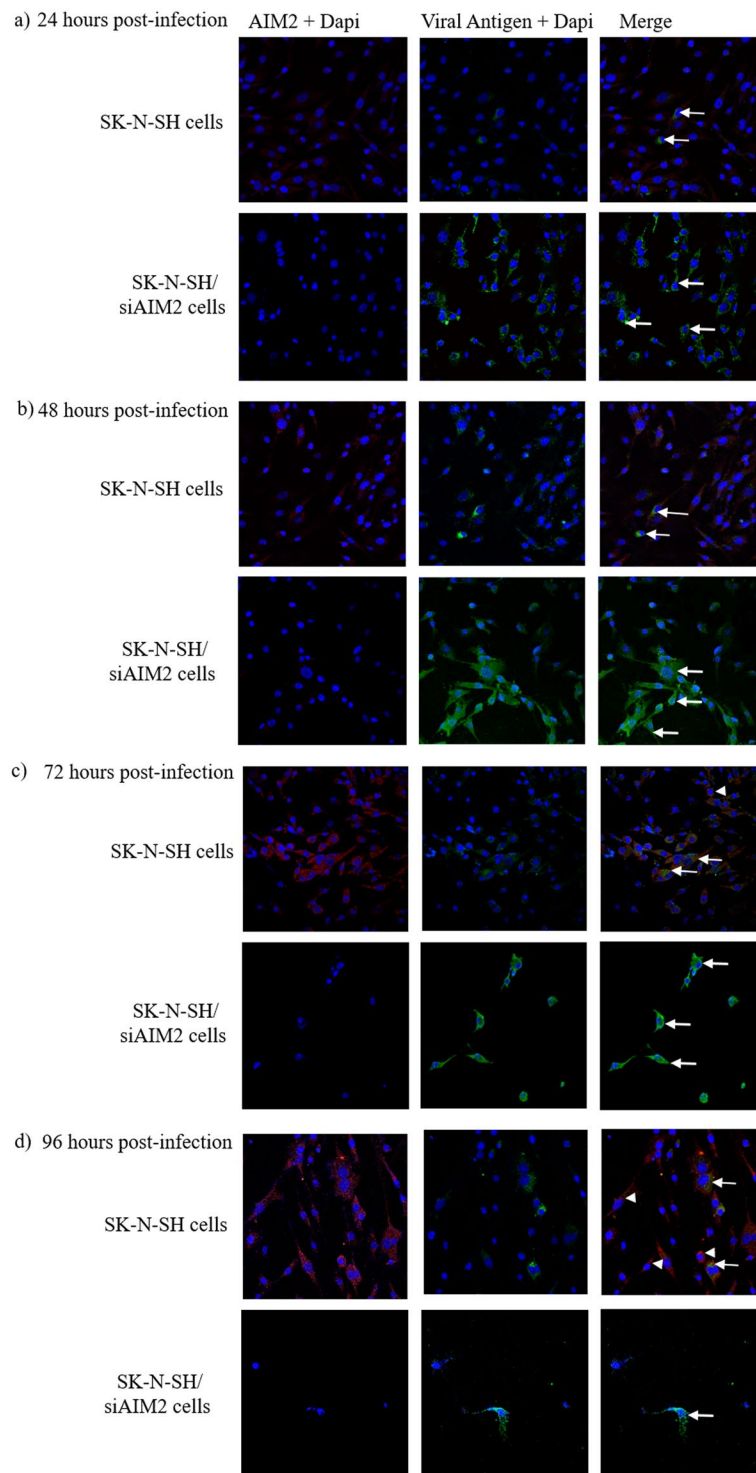


**Figure 6.** Viral infection induced AIM2 and pyroptosis in SK-N-SH cells but not in SK-N-SH/siAIM2 cells. EV-A71/13903-infected SK-N-SH cells and SK-N-SH/siAIM2 cells at 24 (a), 48 (b), 72 (c) and 96 hpi (d), stained for viral antigens (green), AIM2 (red) and dapi (blue, nuclear staining). Viral antigen-positive SK-N-SH cells were also positive for AIM2 (a–d, white arrows) for all time points. At 72 and 96 hpi but not at earlier time points, viral antigen-negative cells stained positive for AIM2 (c,d, white arrowheads). SK-N-SH/siAIM2 cells showed extensive viral antigen staining ((a–d), white arrows) without AIM2 expression for all time points. Magnification 20x.

AIM2 up-regulation was validated by RT-qPCR, which showed a marked increase of AIM2 gene expressions in all 3 EV-A71 strains (Figs 2 and 3a). AIM2 protein was detected in infected SK-N-SH cells of (Figs 3a and

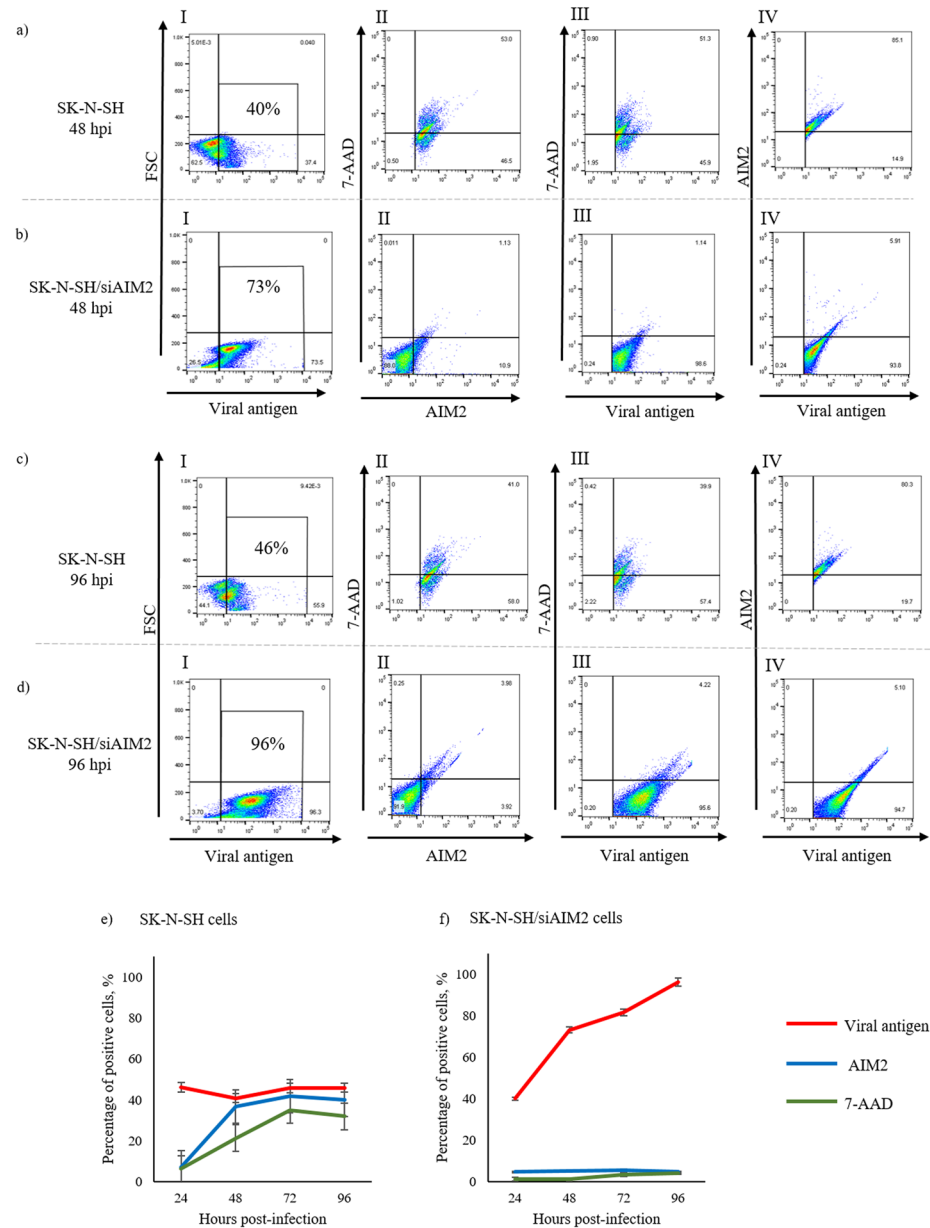


**Figure 7.** AIM2 induced pyroptosis limited viral replication in infected SK-N-SH but not in SK-N-SH/siAIM2 cells. Flow cytometry analysis of viral antigens, AIM2 expression and 7-AAD staining in infected SK-N-SH and SK-N-SH/siAIM2 cells as acquisition plots, at 48 (**a,b**) and 96 (**c,d**) hours post-infection (hpi), and as percentage graphs at 24, 48, 72 and 96 hpi (**e,f**). (**a,b**) At 48 hpi, viral antigen-positive SK-N-SH cells at about 40% (**a,I**) was significantly lower ( $p = 0.0002$ ) compared to SK-N-SH/siAIM2 cells at about 73% (**b,I**). SK-N-SH cells with viral antigen, AIM2 and 7-AAD positivity at about 53% (**a,II**) was significantly much higher ( $p = 0.0002$ ) than in SK-N-SH/siAIM2 cells, which was about 1% (**b,II**). Among viral antigen-positive SK-N-SH cells, 7-AAD positivity of about 51% (**a,III**) was significantly much higher ( $p = 0.0001$ ) than in SK-N-SH/siAIM2 cells which was about 1% (**b,III**). Similarly, among viral antigen-positive SK-N-SH cells, AIM2 positivity was significantly much higher ( $p = 0.003$ ) at about 85% (**a,IV**) than in SK-N-SH/siAIM2 cells, which was about 6% (**b,IV**). (**c,d**) A similar pattern was observed in SK-N-SH cells at 96 hpi, in which viral antigen-positivity (about 46%) (**c,I**) was significantly higher ( $p = 0.0009$ ) than in SK-N-SH/siAIM2 cells (about 96%) (**d,I**). SK-N-SH cells with viral antigen, AIM2 and 7-AAD positivity (about 41%) (**c,II**) were significantly much higher ( $p = 0.001$ ) than SK-N-SH/siAIM2 cells (about 4%) (**d,II**). The same pattern of significantly much higher ( $p = 0.001$ ) viral antigen/7-AAD positive SK-N-SH cells (**c,III**), and significantly much higher ( $p = 0.006$ ) viral antigen/AIM2 positive cells (**c,IV**) compared to SK-N-SH/siAIM2 cells (**d,III** and **d,IV**) was also observed. (**e**) The percentage of AIM2 and 7-AAD-positivity in SK-N-SH cells, showed significant increase ( $p = 0.003$  and  $p = 0.0005$ , respectively) from 24 to 48 hpi but the percentage of viral antigen-positive cells did not increase at these and later time points. (**f**) In contrast, AIM2 and 7-AAD-positive SK-N-SH/siAIM2 cells were below 6% for all time points, while a sharp and significant increase of viral antigen-positive cells was observed from 24 hpi onwards ( $p = 0.007$ , 0.03 and 0.04 at 48, 72 and 96 hpi, respectively). All data represent the mean  $\pm$  standard deviation of a set of triplicates.



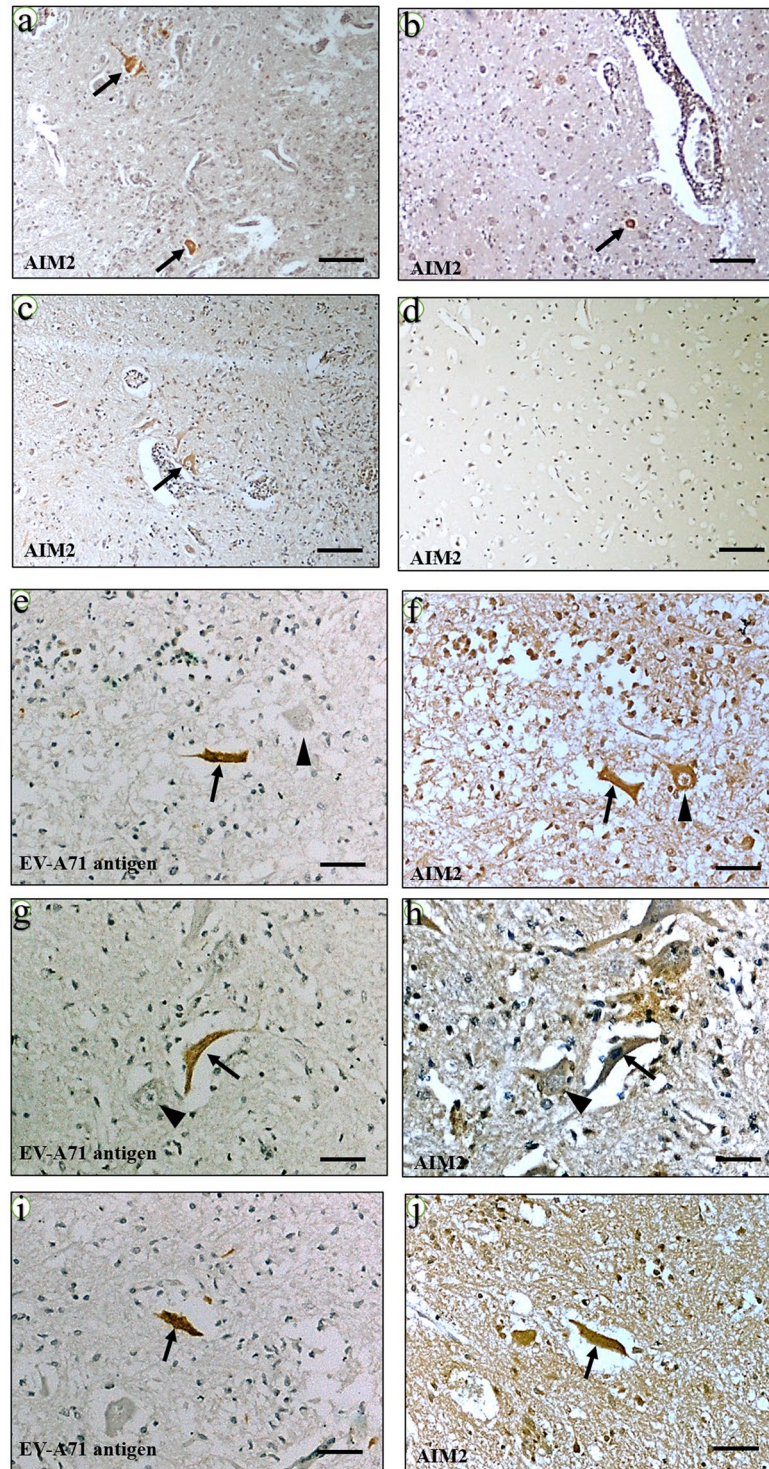


**Figure 8.** AIM2 antigens was expressed in inflamed areas and EV-A71-infected neurons in human encephalomyelitis. AIM2 was positive in inflamed areas of the spinal cord (**a,b**) and medulla (**c**) (arrows). In the respective, immediately adjacent spinal cord tissue sections, viral antigens ((**e,g,i**) arrows) and AIM2 ((**f,h,j**) arrows) were positive in the same neurons. Some neurons were AIM2 positive but viral antigen negative ((**e,f,g,h**) arrowheads). The cerebral cortex (**d**) and other uninflamed areas were negative for AIM2 and viral antigens. Immunohistochemistry using DAP and counter stained with hematoxylin. Magnification 20x (**a–d**) and 20x (**e–j**). Scale bar = 100  $\mu\text{m}$  (**a–d**) and 50  $\mu\text{m}$  (**e–j**).

6a–d and 7a and c), while totally absent in mock-infected cells at the 72 hpi (Figs 3a and S3). As part of the AIM2 inflammasome assembly and pyroptosis pathway, CARD16 and caspase-1 up-regulation (Table 1) were also

confirmed by RT-qPCR for all time points (Fig. 3). Activated caspase-1 (cleaved caspase-1 p20 subunits)<sup>46</sup>, was detected only in infected cells (Fig. 3b). Interestingly, even though IL-1 $\beta$  was not shown to be highly up-regulated in the transcriptome analysis (Table 1), the RT-qPCR confirmed its up-regulation at all time points (Fig. 3e). However, IL-18 was not detected by transcriptome analysis. Infected SK-N-SH/siAIM2 showed about 50–85% AIM2 reduction (Fig. 3a) resulting in corresponding and significant decreases of CARD16 (Fig. 3d), caspase-1 (Fig. 3b) and IL-1 $\beta$  (Fig. 3e) expressions. In agreement with AIM2 up-regulation in infected SK-N-SH cells, AIM2 protein was detected in neurons and inflammatory cells in human EV-A71 encephalomyelitis (Fig. 8). AIM2-positive neurons were exclusively found in areas where EV-A71 antigens and/or intense inflammation were observed<sup>20,64</sup>, suggesting that AIM2 was only highly expressed in infected and inflamed areas of the CNS.

Our results showed that AIM2-positive, infected SK-N-SH cells were highly positive for 7-AAD (Fig. 7a and c) and increased proportionately with AIM2 expression (Fig. 7e). Conversely, infected SK-N-SH/siAIM2 cells showed a significantly lower proportion of 7-AAD-positive cells (Fig. 7b,d and f). Loss of cell membrane integrity during pyroptosis enables 7-AAD to readily permeate into cells, thus this dye has been used as a marker to distinguish programmed cell death by pyroptosis from apoptosis<sup>41,65</sup>. In addition, pyroptotic cell swelling widely observed in infected SK-N-SH cells (Fig. 5a) but not in infected SK-N-SH/siAIM2 cells (Fig. 5c), correlated well with 7-AAD staining of infected cells (Fig. 5b and d). Taken together, these results suggest that EV-A71 infection triggered AIM2 expression and AIM2-mediated up-regulation of specific genes leading to pyroptosis and neuronal cell death.

Our data strongly indicates that AIM2 inflammasome upregulation and pyroptosis suppresses EV-A71 infection and replication in neurons. Increased AIM2 expression at early time points (Figs 3a and 7e) was associated with a significant reduction in viral copy numbers after 24 hpi (Fig. 3c) and suppression of viral titer increase after 48 hpi (Fig. 4). Furthermore, there were reduced viral antigen-positive cells at 72 and 96 hpi (Fig. 6c and d). On the other hand, compared to SK-N-SH cells, infected SK-N-SH/siAIM2 cells generally showed significantly higher viral RNA copies (Fig. 3c), viral titers (Fig. 4), proportion of viral antigen-positive cells (Fig. 7f), and higher expressions of viral antigens by IF (Fig. 6a–d) and flow cytometry (Fig. 7b,d and f) for all time points. Interestingly, at 24 hpi even though AIM2 mRNA expression in SK-N-SH and SK-N-SH/siAIM2 cells (Fig. 3a) was the highest, viral copies remained highest suggesting AIM2 takes effect thereafter. Furthermore, we believe that knock-down of AIM2 expression takes effects only after 48 hpi and the partial AIM2 mRNA levels present at 24 hpi in SK-N-SH/siAIM2 cells (Fig. 3a) may still be sufficient to suppress viral copies which explains the significant reduction from 24 to 48 hpi (Fig. 3c). However, from 48 hpi onwards, when AIM2 reduction was lowest and constant in SK-N-SH/siAIM2 cells, viral copies actually increased ( $p < 0.05$ ) (Fig. 3c). This is in agreement with viral titers in SK-N-SH/siAIM2 cells where a substantial increase was observed only after 48 hpi (Fig. 4). Nonetheless, apart from AIM2, other unknown factors/mechanisms may also contribute to viral suppression. Decreasing viral replication in SK-N-SH cells and increasing viral replication in SK-N-SH/siAIM2 cells at later time points were strongly associated with the significant increase and decrease, respectively, with 7-AAD positivity (Fig. 7e–f). This suggests that AIM2 inflammasome-mediated pyroptosis may play an important role in limiting EV-A71 replication in general as both mild HFMD and fatal encephalomyelitis viral isolates could infect neuronal cells and up-regulate AIM2 expression (Fig. 2). This idea is analogous to the recognition that infected non-inflammatory host cells undergo apoptosis leading to premature cell death and limitation of intracellular virus propagation and spread<sup>66,67</sup>. It has been shown that *in vitro* and *in vivo* WNV-induced neuronal apoptosis limited CNS injury, viral replication and dissemination<sup>68,69</sup>. Similarly, in vesicular stomatitis virus infection, apoptosis limited viral replication through involvement of perforin and granzymes<sup>70</sup>. Chikungunya virus and WNV infection in human dermal fibroblast cells have been reported to activate caspase-1 which limited viral replication, but the authors did not associate these findings with pyroptosis<sup>56</sup>. To our knowledge, pyroptosis as a cell death mechanism that could limit viral replication and dissemination has not been reported before. A previous study on *Burkholderia pseudomallei* showed that caspase-11 induced pyroptosis could inhibit intracellular bacterial growth<sup>62</sup> even though there was no release of IL-1 $\beta$ . Our findings and hypothesis should be further investigated using primary human neuronal cultures and animal models including AIM2-knockout mouse models, which have been previously shown to increase murine cytomegalovirus virus replication<sup>55</sup>.

Pyroptosis releases activated IL-1 $\beta$  and other pro-inflammatory cytokines eventually leading to limitation of infection<sup>40,71</sup>. In murine cytomegalovirus and vaccinia virus infections in macrophage cultures and mouse models, AIM2 inflammasome-associated pyroptosis has been described, and activated IL-1 $\beta$  was thought to play a critical role in host innate immunity against infection<sup>72–74</sup>. In our study, we showed significant increase in IL-1 $\beta$  expression by RT-qPCR (Fig. 3e), consistent with pyroptosis. Hence, apart from macrophages, neutrophils and NK cells, our results suggested that virus-infected neuronal cells may also up-regulate IL-1 $\beta$  to recruit immune cells, including NK cells, to the site of infection, and to trigger IFN- $\gamma$  production. Interestingly, in an EV-A71 infection mouse model, viral proteases were able to overcome the effects of NLRP3 inflammasome activated IL-1 $\beta$  leading to increased viral replication<sup>75</sup>. Hence, the role of AIM2 inflammasome activated IL-1 $\beta$  in EV-A71 infections needs to be further investigated. We also showed increase of tumour necrosis factor, IL-6 and CXCL10 in the transcriptomic analysis (Table 1 and Supplementary Figure S4), which were also found in the cerebrospinal fluids of EV-A71 encephalomyelitis patients<sup>76–79</sup>. It is possible that these inflammatory mediators may be released from infected CNS neurons as part of pyroptosis.

Our study showed that AIM2 inflammasome assembly could be triggered by cytosolic EV-A71 RNA while previously it was mostly described in cytosolic DNAs<sup>80</sup>. We also showed AIM2 gene up-regulation and activation following viral RNA transfection of SK-N-SH cells (Fig. 3f). However, UV-inactivated viral RNA failed to trigger AIM2 (Fig. 3f) and caspase-1 (Fig. 3g) up-regulation possibly because of photochemical damage to genomic RNA<sup>81–83</sup>, suggesting that UV damaged RNA may not activate AIM2 inflammasome. However, the detailed mechanisms by which AIM2 specifically detects and interacts with EV-A71 RNA is unknown. In the presence of cytosolic DNAs, AIM2 is known to bind DNA directly through its ASC via its pyrin domain<sup>84</sup> and the

Virus designation	Passage number	Year of isolation	Disease/Isolation site	Gene accession number
EV-A71/13903	6	1997	Fatal HFMD/medulla oblongata	AY207648
EV-A71/18431	3	2006	Fatal HFMD/throat	NA
EV-A71/SB12736	3	2003	HFMD/NA	AY794025

**Table 2.** Virus strains used in experiments. \*NA – not available; HFMD – Hand, foot and mouth disease

two adjacent oligonucleotide/oligosaccharide-binding folds in the C-terminal HIN-200 domain<sup>63</sup>. Even though, AIM2 up-regulation has been described in Chikungunya virus and WNV infections in human fibroblast cells, the ability of viral RNAs to trigger AIM2 up-regulation was not investigated<sup>56</sup>. In conclusion, we found that EV-A71 infection of neuronal cells induced up-regulation of AIM2 and inflammasome assembly leading to pyroptosis cell death and suppression of viral replication.

## Materials and Methods

**Virus and cells.** All EV-A71 strains used in this study were clinical isolates (Table 2). The viruses were grown and titrated in Vero cells by the cell culture infectious dose 50 (CCID<sub>50</sub>) assay as described previously<sup>85, 86</sup>. Vero (ATCC-CCL-81) and SK-N-SH (ATCC-HTB-11) cell lines were propagated in Dulbecco's modified Eagle's medium, supplemented with 5% and 10% fetal bovine serum, respectively. Rhabdomyosarcoma cells (ATCC-CCL-136) were propagated in Roswell Park Memorial Institute medium, supplemented with 10% fetal bovine serum, and used as positive controls in the double immunofluorescence assay. All assays using SK-N-SH cells were done in triplicates, and all procedures using commercial kits/reagents followed manufacturers' protocols unless stated otherwise.

**EV-A71 infection of SK-N-SH cells.** SK-N-SH cells in 2 ml microcentrifuge tubes were infected with EV-A71/13903 at a multiplicity of infection (MOI) of 10 for all experiments unless otherwise stated. After keeping in a shaking incubator at 37 °C for 2 hours followed by centrifugation at 400 × g, the cell pellet was washed twice with phosphate-buffered saline (PBS) before re-suspension in 500 µl of culture medium and seeding into 24-well plates. After incubation at 37 °C, infected cells and supernatant were harvested at 24, 48, 72 and 96 hours post-infection (hpi) for flow cytometry studies, and RNA extraction for microarray and quantitative real-time PCR analysis. Mock-infected cells/RNA as negative controls were prepared following the same procedure.

**Flow cytometry.** *Quantitation of viral antigens in infected SK-N-SH cells.* Flow cytometry was used to quantify the proportion of infected SK-N-SH cells by viral antigen detection. Briefly, infected and mock-infected cells were trypsinized and centrifuged at 400 × g in 1.5 ml microcentrifuge tubes. Cell pellets were fixed with Fluorofix buffer (Biolegend, USA) for 30 min at room temperature (RT) in the dark<sup>87–89</sup>, and PBS-washed twice before permeabilization with 0.005% Triton-X100 for 10 min. Cells were then incubated for 1 hr at RT with mouse monoclonal Enterovirus blend 3321 antibody (dilution 1:50; Merck, Germany), followed by goat-anti mouse IgG conjugated with Alexa-fluor 488 (Molecular Probes, USA) for 30 min at RT in the dark<sup>90</sup>. Cells were re-suspended in cell staining buffer (Biolegend, USA) before analysis using the FACS Canto II Flow cytometer (Becton Dickson, USA) and the FlowJo, Single Cell Analysis Software version 10 (FlowJo, USA).

*Co-localization of viral antigens with AIM2 or 7-amino-actinomycin in infected SK-N-SH cells.* EV-A71/13903-infected SK-N-SH and AIM2-knockdown SK-N-SH cells (SK-N-SH/siAIM2) cells at MOI of 1, and mock-infected cells were triple-stained for EV-A71 antigens, AIM2 and 7 amino-actinomycin (7-AAD). Previously shown to be useful as a biomarker for pyroptosis, 7-AAD is able to enter nuclear membranes to stain DNA following the loss of membrane integrity<sup>41, 65, 91</sup>. Briefly, infected and mock-infected cells were collected in 1.5 ml microcentrifuge tubes and incubated for 5 minutes with 7-AAD<sup>87–89</sup>. The cell pellets were then fixed with Fluorofix buffer and stained for viral antigen and AIM2 protein were using mouse monoclonal Enterovirus blend 3321 antibody and rabbit polyclonal AIM2 K-12 antibody (dilution 1:500; Santa Cruz, USA), followed by incubation with by goat-anti mouse IgG conjugated with Alexa-fluor 488 and goat anti-rabbit IgG conjugated with Alexa-fluor 546 (Molecular Probes, USA) for 30 min at RT in the dark<sup>92</sup>. Flow cytometry analysis to assess localization of viral antigens and AIM2 or 7-AAD was performed as before.

*Assessment of transfection efficiency and 7-AAD staining in viral RNA transfected SK-N-SH cells.* Transfection efficiency was assessed by flow cytometry after transfection of 75 pmol siGLO Green Transfection Indicator (D-001630-01-20; Dharmacon, USA) in treated and untreated SK-N-SH cells at 48 h post-transfection (hpt). To assess 7-AAD staining, SK-N-SH cells were incubated with 7-AAD for 5 minutes at RT before fixation in Fluorofix buffer and flow cytometry analysis.

**Transcriptome analysis of infected SK-N-SH cells.** Total RNA was extracted from infected and mock-infected SK-N-SH cells at the 48 and 72 hpi using the RNeasy Plus Mini kit (Qiagen, Germany). Biotinylated cRNA were prepared and fragmented from 100 ng total RNA (GeneChip 3' IVT Express Array, 2008–2010, Affymetrix), followed by hybridization of 12 µg of cRNA for 16 hr at 45 °C on the GeneChip. After washing and staining using the Affymetrix® GeneChip® Fluidics Station 450, the GeneChip was scanned using the GeneChip® Scanner 3000. Data were analyzed with the Expression console software (default analysis settings

and the RMA processing algorithm). Statistical tests for gene level differential expression were performed using the Transcriptome Analysis Console (TAC) v2.0 software. All data sets were deposited into the Gene Expression Omnibus (Gene accession: GSE71673) using MIAME guidelines. Further analysis of gene expression and pathways was done by the IPA software (Ingenuity® Systems, <http://www.ingenuity.com/>).

**Real time quantitative PCR (RT-qPCR) of viral RNA and selected genes in infected SK-N-SH cells.** To quantify viral RNA copies, Taqman primers (EV-A71-F: GCACAACCTCACCATTGGA, EV-A71-R: GCTGTAGCATCGTCATCA) and probe (FAM-CACCATTACTACACAGGAGGCGGC-TAMRA) were used. Total RNA was extracted from EV-A71/13903, EV-A71/18431 and EV-A71/SB12736 infected and mock-infected SK-N-SH cells at the 24, 48, 72 and 96 hpi using the RNeasy Plus kit (Qiagen, Netherlands). The cDNA template (1 µg), prepared using the iScript cDNA synthesis kit (Biorad, USA), was mixed with Taqman advance fast master mix (Applied Biosystem, USA), Taqman primers and probe. The cycling conditions were denaturation at 95 °C for 5 sec, amplification and quantification for 45 cycles at 95 °C for 30 s and 60 °C for 10 s, using the ABI 7500 fast real-time PCR system (Applied Biosystem, USA). The results were analyzed using the 7500 Software version 2.0.6. (Applied Biosystem, USA).

Based on transcriptome analysis results, selected genes of interest, AIM2 (Hs00915710), caspase-1 (Hs00354836), CARD 16 (Hs03008439), and IL-1β (Hs00174097), were further investigated by RT-qPCR using commercially-available Taqman assays/reagents (Applied Biosystem, USA) and conditions, as described. Hypoxanthine phosphoribosyltransferase 1 (HPRT1; Hs02800695) and succinate dehydrogenase complex flavo-protein subunit A (SDHA; Hs00188166) were used as internal controls. Glyceraldehyde 3-phosphate dehydrogenase (GAPDH; Hs02786624) was used as siRNA control.

**AIM2 and caspase-1 gene expressions, and viral copy number quantitation in viral RNA transfected SK-N-SH cells.** To study AIM2 and caspase-1 gene expressions following viral RNA transfection, SK-N-SH cells ( $5 \times 10^4$  cells/ml) were seeded into 24-well plates at 37 °C overnight before transfection with 200 ng of EV-A71/13903 viral RNA and UV-inactivated EV-A71/13903 viral RNA using Lipofectamine 2000 (Invitrogen, USA). Total RNA were extracted from transfected and mock-transfected cells at 12 and 24 hpt and RT-qPCR was performed as before. Viral RNA was inactivated by ultraviolet (UV) light as described previously<sup>93</sup>. Briefly, PBS-diluted virus stock was exposed to UV light for 30 minutes, and viral RNA extracted using High pure viral RNA extraction kit (Roche, Switzerland). Successful viral RNA inactivation was determined by absence of CPE and negative virus isolation in transfected Vero cells after 7 days. The transfection efficiency of Lipofectamine 2000 into cells was determined using 200 ng of Monster Green Fluorescent expression vector, mGFP (Promega, USA).

**AIM2 gene knockdown in SK-N-SH cells and EV-A71 infection.** To further investigate its role in EV-A71 infection, AIM2 in SK-N-SH cells was silenced using Silencer® Select AIM2 siRNA (s18093; Ambion, USA) before infection. Briefly, SK-N-SH cells ( $5 \times 10^4$  cells/ml) were seeded into 24-well plates at 37 °C overnight, before transfection with 75 pmol siRNA using RNAimax (Invitrogen, USA). At 48 hpt, SK-N-SH/siAIM2 cells were infected with EV-A71/13903. Cells were collected at 24, 48, 72 and 96 hpi for RT-qPCR to quantitate AIM2, CARD16, caspase-1 and IL-1β mRNA expression and viral RNA copies. Cells at 72 hpi were collected for Western blot analysis of these proteins. Silencer select GAPDH gene (Ambion, USA) and Silencer select Negative controls (Ambion, USA) were used as positive and negative internal controls, respectively. Transfection efficiency and cell viability post-transfection were analyzed using flow cytometry as before.

**Western blot analysis of AIM2 protein.** After 72 hpi, infected and mock-infected SK-N-SH and SK-N-SH/siAIM2 cells were rapidly washed with ice-cold PBS, scraped and centrifuged at 1000 × g for 10 min. Total proteins were extracted using Protein EX cell lysis buffer (GeneAll, Korea) supplemented with a phosphatase inhibitor, Pierce phosphatase inhibitor mini table (Thermo, USA) to prevent protein degradation and preserve their activation states. Protein concentration was determined by the Pierce BCA reagents (Thermo, USA), and 20 µg protein supernatant fractions were denatured and subjected to SDS-PAGE as described previously<sup>94</sup>, with minor modifications. Briefly, the polyvinylidene fluoride membrane was incubated with AIM2 K-12 antibody (dilution 1:250; Santa Cruz, USA), Pierce EV-A71 Antibody (dilution 1:40000; Thermo, USA), caspase-1 antibody (dilution 1:100; Cell Signaling, USA), and HPRT1 antibody (dilution 1:500; Thermo, USA), respectively, overnight at 4 °C. Secondary goat anti-mouse IgG (31322) and goat anti-rabbit IgG (31342) antibodies conjugated with alkaline phosphatase (dilution 1:20000; Thermo, USA) were sequentially added. Blots were developed using 1-Step NBT/BCIP (Thermo, USA) at RT.

**Double immunofluorescence (IF) to detect AIM2 and viral antigens.** Double IF was performed to co-localize of AIM2 and viral antigens in infected SK-N-SH and SK-N-SH/siAIM2. Approximately,  $5 \times 10^4$  cells were seeded onto Lab-Tek 8-well chamber slides (Nunc, Denmark) for 24 hours before infection with EV-A71/13903 for 2 hours at 37 °C. Infected and mock-infected cells were then fixed with methanol for 10 min at -20 °C and incubated with primary antibodies (AIM2-K12, dilution 1:500 and Enterovirus blend 3321, dilution 1:50) diluted in Tris-buffered-saline (TBS, pH 7.6) overnight at 4 °C. Secondary antibody staining as described before in the flow cytometry analysis, followed by DAPI counter staining was done before mounting in fluorescence mounting medium (Dako, Denmark). All the stained slides were analyzed using TCS SP5 II, Leica confocal laser scanning microscope (Leica, Germany). Normal human small intestine tissues were used as positive controls for AIM2. EV-A71/13903-infected Rhabdomyosarcoma cells served as positive controls.

**Immunohistochemistry (IHC) to detect viral antigens and AIM2 protein in human EV-A71 encephalomyelitis.** The CNS tissues of 3 confirmed EV-A71 encephalomyelitis cases from a previous autopsy series<sup>22, 95</sup> were investigated by IHC for AIM2 protein expression. IHC was performed by a standard ENVISION technique as described previously<sup>96</sup>. Briefly, deparaffinized and rehydrated tissue sections were endogenous peroxidase blocked before antigen retrieval at 30 min in Tris-EDTA buffer (pH 9) with 0.05% Tween-20. Tissue sections were then incubated with 10% normal goat serum before incubation overnight at 4 °C with mouse monoclonal Enterovirus blend 3321 antibody (dilution 1:50; Merck, Germany) or rabbit polyclonal AIM2 K-12 antibody (dilution 1:500; Santa cruz, USA). Secondary goat-anti mouse IgG HRP-conjugated (Dako, Denmark) or goat-anti rabbit IgG HRP conjugated (Dako, Denmark) respectively, was applied, followed by DAB (Dako, Denmark) chromogen. The slides were counterstained with hematoxylin (Dako, Denmark) and mounted with DPX mounting medium (Sigma, USA). Negative controls for IHC were normal human brain tissues. Positive controls for AIM2 staining were normal human small intestine and for EV-A71 antigens, EV-A71/13903 infected SK-N-SH cells. Duplicate assays on test tissues were also done by replacing the primary antibodies with isotype control antibodies or normal rabbit immunoglobulin fractions (I) (Dako, Denmark).

**Statistical analysis.** Data was reported as mean  $\pm$  standard deviation of at least three independent experiments performed. The unpaired student t-test in the Statistical Package for the Social Sciences (SPSS) was used to calculate p values. P values of  $\leq 0.05$  were considered significant.

**Ethics statement.** All samples used in the experiments were from an already-existing collection and anonymized. The EV-A71/13903 virus ethics approval were obtained from Faculty of Medicine, Institutional Animal Care and Use Committee, University of Malaya (Ethics reference no: 2014-02-14/PATH/R/WKT). The viruses EV-A71/18431 and EV-A71/SB12736 were part of a HFMD surveillance program in collaboration of Sarawak Health Department with The Institute of Health and Community Medicine, University of Malaysia Sarawak where the Malaysia samples were given for research purposes. As such, an ethics or IRB approval was not needed.

## References

1. WHO. <http://www.wpro.who.int/publications/docs/GuidancefortheclinicalmanagementofHFMD.pdf> 71 (World Health Organization, Geneva, Switzerland, 2011).
2. Wang, Q. *et al.* Clinical features of severe cases of hand, foot and mouth disease with EV71 virus infection in China. *Archives of Medical Science: AMS* **10**, 510–516, doi:10.5114/aoms.2014.43745 (2014).
3. Shah, V. A., Chong, C. Y., Chan, K. P., Ng, W. & Ling, A. E. Clinical characteristics of an outbreak of hand, foot and mouth disease in Singapore. *Annals of the Academy of Medicine Singapore* **32**, 381–387 (2003).
4. Schmidt, N. J., Lennette, E. H. & Ho, H. H. An apparently new enterovirus isolated from patients with disease of the central nervous system. *The Journal of infectious diseases* **129**, 304–309 (1974).
5. Blomberg, J. *et al.* Letter: New enterovirus type associated with epidemic of aseptic meningitis and/or hand, foot, and mouth disease. *Lancet* **2**, 112 (1974).
6. Chan, Y. F., Wee, S. I., AbuBakar, K. L. & Enterovirus, S. 71 in Malaysia: A decade later. *Neurology Asia* **16**, 1–15 (2011).
7. Hsueh, C. *et al.* Acute encephalomyelitis during an outbreak of enterovirus type 71 infection in Taiwan: report of an autopsy case with pathologic, immunofluorescence, and molecular studies. *Modern pathology: an official journal of the United States and Canadian Academy of Pathology, Inc* **13**, 1200–1205, doi:10.1038/modpathol.3880222 (2000).
8. NikNadia, N. M. N. *et al.* Cyclical Patterns of Hand, Foot and Mouth Disease Caused by Enterovirus A71 in Malaysia. *PLoS neglected tropical diseases* **10**, e0004562, doi:10.1371/journal.pntd.0004562 (2016).
9. Lin, T. Y., Twu, S. J., Ho, M. S., Chang, L. Y. & Lee, C. Y. Enterovirus 71 outbreaks, Taiwan: occurrence and recognition. *Emerging infectious diseases* **9**, 291–293, doi:10.3201/eid0903.020285 (2003).
10. Shindarov, L. M. *et al.* Epidemiological, clinical, and pathomorphological characteristics of epidemic poliomyelitis-like disease caused by enterovirus 71. *Journal of hygiene, epidemiology, microbiology, and immunology* **23**, 284–295 (1979).
11. Chumakov, M. *et al.* Enterovirus 71 isolated from cases of epidemic poliomyelitis-like disease in Bulgaria. *Archives of virology* **60**, 329–340 (1979).
12. Hagiwara, A., Tagaya, I. & Yoneyama, T. Epidemic of hand, foot and mouth disease associated with enterovirus 71 infection. *Intervirology* **9**, 60–63 (1978).
13. Kennett, M. L. *et al.* Enterovirus type 71 infection in Melbourne. *Bulletin of the World Health Organization* **51**, 609–615 (1974).
14. Lee, T. C. *et al.* Diseases caused by enterovirus 71 infection. *The Pediatric infectious disease journal* **28**, 904–910, doi:10.1097/INF.0b013e3181a41d63 (2009).
15. McMinn, P., Stratov, I., Nagarajan, L. & Davis, S. Neurological manifestations of enterovirus 71 infection in children during an outbreak of hand, foot, and mouth disease in Western Australia. *Clinical Infectious Diseases* **32**, 236–242, doi:10.1086/318454 (2001).
16. He, S. J. *et al.* [Three cases of enterovirus 71 infection with pulmonary edema or pulmonary hemorrhage as the early clinical manifestation]. *Zhonghua er ke za zhi. Chinese journal of pediatrics* **46**, 513–516 (2008).
17. Ooi, M. H., Wong, S. C., Lewthwaite, P., Cardoso, M. J. & Solomon, T. Clinical features, diagnosis, and management of enterovirus 71. *The Lancet Neurology* **9**, 1097–1105, doi:10.1016/S1474-4422(10)70209-X (2010).
18. Liu, K. *et al.* [Neurologic complications in children with enterovirus 71-infected hand-foot-mouth disease: clinical features, MRI findings and follow-up study]. *Zhonghua yi xue za zhi* **92**, 1742–1746 (2012).
19. Chen, F., Li, J. J., Liu, T., Wen, G. Q. & Xiang, W. Clinical and neuroimaging features of enterovirus 71 related acute flaccid paralysis in patients with hand-foot-mouth disease. *Asian Pacific journal of tropical medicine* **6**, 68–72, doi:10.1016/s1995-7645(12)60203-x (2013).
20. Ong, K. C. & Wong, K. T. Understanding Enterovirus 71 Neuropathogenesis and Its Impact on Other Neurotropic Enteroviruses. *Brain Pathology* **25**, 614–624, doi:10.1111/bpa.12279 (2015).
21. Yan, J.-J., Wang, J.-R., Liu, C.-C., Yang, H.-B. & Su, I.-J. An outbreak of enterovirus 71 infection in Taiwan 1998: A comprehensive pathological, virological, and molecular study on a case of fulminant encephalitis. *Journal of Clinical Virology* **17**, 13–22, doi:10.1016/S1386-6532(00)00067-6 (2000).
22. Lum, L. C. *et al.* Fatal enterovirus 71 encephalomyelitis. *The Journal of pediatrics* **133**, 795–798 (1998).
23. Shieh, W. J. *et al.* Pathologic studies of fatal cases in outbreak of hand, foot, and mouth disease, Taiwan. *Emerging Infectious Diseases* **7**, 146–148, doi:10.3201/eid0701.700146 (2001).
24. Fink, S. L. & Cookson, B. T. Apoptosis, pyroptosis, and necrosis: mechanistic description of dead and dying eukaryotic cells. *Infection and immunity* **73**, 1907–1916, doi:10.1128/IAI.73.4.1907-1916.2005 (2005).

25. Zhang, R. *et al.* The regulation of autophagy by influenza A virus. *BioMed research international* **2014**, 498083, doi:10.1155/2014/498083 (2014).
26. Huang, Z. *et al.* RIP1/RIP3 Binding to HSV-1 ICP6 Initiates Necroptosis to Restrict Virus Propagation in Mice. *Cell Host & Microbe* **17**, 229–242, doi:10.1016/j.chom.2015.01.002 (2015).
27. Pan, T. *et al.* Necroptosis Takes Place in Human Immunodeficiency Virus Type-1 (HIV-1)-Infected CD4+ T Lymphocytes. *PLOS ONE* **9**, e93944, doi:10.1371/journal.pone.0093944 (2014).
28. Ramos, H. J. *et al.* IL-1 $\beta$  Signaling Promotes CNS-Intrinsic Immune Control of West Nile Virus Infection. *PLoS pathogens* **8**, e1003039, doi:10.1371/journal.ppat.1003039 (2012).
29. Inoue, H. & Tani, K. Multimodal immunogenic cancer cell death as a consequence of anticancer cytotoxic treatments. *Cell death and differentiation* **21**, 39–49, doi:10.1038/cdd.2013.84 (2014).
30. Chang, S. C., Lin, J. Y., Lo, L. Y., Li, M. L. & Shih, S. R. Diverse apoptotic pathways in enterovirus 71-infected cells. *Journal of neurovirology* **10**, 338–349, doi:10.1080/13550280490521032 (2004).
31. Shih, S. R., Weng, K. F., Stollar, V. & Li, M. L. Viral protein synthesis is required for Enterovirus 71 to induce apoptosis in human glioblastoma cells. *Journal of neurovirology* **14**, 53–61, doi:10.1080/13550280701798980 (2008).
32. Shi, W. *et al.* Differential apoptosis gene expressions of rhabdomyosarcoma cells in response to enterovirus 71 infection. *BMC infectious diseases* **12**, 327, doi:10.1186/1471-2334-12-327 (2012).
33. Chen, T. C., Lai, Y. K., Yu, C. K. & Juang, J. L. Enterovirus 71 triggering of neuronal apoptosis through activation of Abl-Cdk5 signalling. *Cellular microbiology* **9**, 2676–2688, doi:10.1111/j.1462-5822.2007.00988.x (2007).
34. Chan, S. Y., Sam, I. C., Lai, J. K. & Chan, Y. F. Cellular proteome alterations in response to enterovirus 71 and coxsackievirus A16 infections in neuronal and intestinal cell lines. *Journal of proteomics* **125**, 121–130, doi:10.1016/j.jprot.2015.05.016 (2015).
35. Yogarajah, T., Ong, K. C., Perera, D. & Wong, K. T. Enterovirus A71 and coxsackievirus A16 show different replication kinetics in human neuronal and non-neuronal cell lines. *Archives of virology*, doi:10.1007/s00705-016-3157-4 (2016).
36. Chan, K. P. *et al.* Epidemic Hand, Foot and Mouth Disease Caused by Human Enterovirus 71, Singapore. *Emerging Infectious Diseases* **9**, 78–85, doi:10.3201/eid1301.020112 (2003).
37. Wei, D., Li, K. X. & Chen, E. [Autopsy report of two cases with enterovirus type 71 infection brainstem encephalitis and literature review]. *Zhonghua er ke za zhi. Chinese journal of pediatrics* **48**, 220–223 (2010).
38. Lu, M. *et al.* [Pathology of enterovirus 71 infection: an autopsy study of 5 cases]. *Zhonghua bing li xue za zhi Chinese journal of pathology* **38**, 81–85 (2009).
39. Adamczak, S. E. *et al.* Pyroptotic neuronal cell death mediated by the AIM2 inflammasome. *Journal of cerebral blood flow and metabolism: official journal of the International Society of Cerebral Blood Flow and Metabolism* **34**, 621–629, doi:10.1038/jcbfm.2013.236 (2014).
40. Bergsbaken, T., Fink, S. L. & Cookson, B. T. Pyroptosis: host cell death and inflammation. *Nat Rev Micro* **7**, 99–109 (2009).
41. Fink, S. L. & Cookson, B. T. Caspase-1-dependent pore formation during pyroptosis leads to osmotic lysis of infected host macrophages. *Cellular microbiology* **8**, 1812–1825, doi:10.1111/j.1462-5822.2006.00751.x (2006).
42. Cunha, L. D. & Zamboni, D. S. Subversion of inflammasome activation and pyroptosis by pathogenic bacteria. *Frontiers in cellular and infection microbiology* **3**, 76, doi:10.3389/fcimb.2013.00076 (2013).
43. Eichholz, K., Bru, T., Tran, T. T., Fernandes, P. & Welles, H. Immune-Complexed Adenovirus Induce AIM2-Mediated Pyroptosis in Human Dendritic Cells. **12**, e1005871, doi:10.1371/journal.ppat.1005871 (2016).
44. Ito, M., Yanagi, Y. & Ichinohe, T. Encephalomyocarditis virus viroporin 2B activates NLRP3 inflammasome. *PLoS pathogens* **8**, e1002857, doi:10.1371/journal.ppat.1002857 (2012).
45. Triantafilou, K., Kar, S., van Kuppeveld, F. J. & Triantafilou, M. Rhinovirus-induced calcium flux triggers NLRP3 and NLRC5 activation in bronchial cells. *American journal of respiratory cell and molecular biology* **49**, 923–934, doi:10.1165/rcmb.2013-0032OC (2013).
46. Denes, A., Lopez-Castejon, G. & Brough, D. Caspase-1: is IL-1 just the tip of the ICEberg? *Cell death & disease* **3**, e338, doi:10.1038/cddis.2012.86 (2012).
47. Freeman, L. C. & Ting, J. P. The pathogenic role of the inflammasome in neurodegenerative diseases. *Journal of neurochemistry* **136**(Suppl 1), 29–38, doi:10.1111/jnc.13217 (2016).
48. Denes, A. *et al.* AIM2 and NLRC4 inflammasomes contribute with ASC to acute brain injury independently of NLRP3. *Proceedings of the National Academy of Sciences of the United States of America* **112**, 4050–4055, doi:10.1073/pnas.1419090112 (2015).
49. Case, C. L. Regulating caspase-1 during infection: roles of NLRs, AIM2, and ASC. *The Yale journal of biology and medicine* **84**, 333–343 (2011).
50. Sagulenko, V. *et al.* AIM2 and NLRP3 inflammasomes activate both apoptotic and pyroptotic death pathways via ASC. *Cell death and differentiation* **20**, 1149–1160, doi:10.1038/cdd.2013.37 (2013).
51. Sollberger, G., Strittmatter, G. E., Garstkiewicz, M., Sand, J. & Beer, H. D. Caspase-1: the inflammasome and beyond. *Innate immunity* **20**, 115–125, doi:10.1177/1753425913484374 (2014).
52. Sauer, J. D. *et al.* *Listeria monocytogenes* triggers AIM2-mediated pyroptosis upon infrequent bacteriolysis in the macrophage cytosol. *Cell host & microbe* **7**, 412–419, doi:10.1016/j.chom.2010.04.004 (2010).
53. Chien, H. & Dix, R. D. Evidence for multiple cell death pathways during development of experimental cytomegalovirus retinitis in mice with retrovirus-induced immunosuppression: apoptosis, necroptosis, and pyroptosis. *Journal of virology* **86**, 10961–10978, doi:10.1128/jvi.01275-12 (2012).
54. Fernandes-Alnemri, T. *et al.* The AIM2 inflammasome is critical for innate immunity to Francisella tularensis. *Nature immunology* **11**, 385–393, [http://www.nature.com/ni/journal/v11/n5/supinfo/ni.1859\\_S1.html](http://www.nature.com/ni/journal/v11/n5/supinfo/ni.1859_S1.html) (2010).
55. Rathinam, V. A. *et al.* The AIM2 inflammasome is essential for host defense against cytosolic bacteria and DNA viruses. *Nature immunology* **11**, 395–402, doi:10.1038/ni.1864 (2010).
56. Ekchariyawat, P. *et al.* Inflammasome signaling pathways exert antiviral effect against Chikungunya virus in human dermal fibroblasts. *Infection, Genetics and Evolution* **32**, 401–408, doi:10.1016/j.meegid.2015.03.025 (2015).
57. Lupfer, C., Malik, A. & Kanneganti, T.-D. Inflammasome control of viral infection. *Current opinion in virology* **12**, 38–46, doi:10.1016/j.coviro.2015.02.007 (2015).
58. Broz, P. & Dixit, V. M. Inflammasomes: mechanism of assembly, regulation and signalling. *Nat Rev Immunol* **16**, 407–420, doi:10.1038/nri.2016.58 (2016).
59. Karasawa, T. *et al.* Oligomerized CARD16 promotes caspase-1 assembly and IL-1 $\beta$  processing. *FEBS Open Bio* **5**, 348–356, doi:10.1016/j.fob.2015.04.011 (2015).
60. Miao, E. A., Rajan, J. V. & Aderem, A. Caspase-1-induced pyroptotic cell death. *Immunological reviews* **243**, 206–214, doi:10.1111/j.1600-065X.2011.01044.x (2011).
61. Arend, W. P., Palmer, G. & Gabay, C. IL-1, IL-18, and IL-33 families of cytokines. *Immunological reviews* **223**, 20–38, doi:10.1111/j.1600-065X.2008.00624.x (2008).
62. Ceballos-Olvera, I., Sahoo, M., Miller, M. A., Del Barrio, L. & Re, F. Inflammasome-dependent pyroptosis and IL-18 protect against *Burkholderia pseudomallei* lung infection while IL-1 $\beta$  is deleterious. *PLoS pathogens* **7**, e1002452, doi:10.1371/journal.ppat.1002452 (2011).
63. Fernandes-Alnemri, T., Yu, J.-W., Wu, J., Datta, P. & Alnemri, E. S. AIM2 activates the inflammasome and cell death in response to cytoplasmic DNA. *Nature* **458**, 509–513, doi:10.1038/nature07710 (2009).

64. Wong, K. T. & KC, O. N. Infectious Diseases and Tropical Disease Pathology: SS16-1 Understanding enterovirus 71 infection and neuropathogenesis: perspective from human and animal model studies. *Pathology* **46**(Suppl 2), S26, doi:10.1097/01.PAT.0000454140.94403.23 (2014).
65. Miao, E. A., Rajan, J. V. & Aderem, A. Caspase-1 induced pyroptotic cell death. *Immunological reviews* **243**, 206–214, doi:10.1111/j.1600-065X.2011.01044.x (2011).
66. Thomson, B. J. Viruses and apoptosis. *International Journal of Experimental Pathology* **82**, 65–76, doi:10.1111/j.1365-2613.2001.iep0082-0065-x (2001).
67. Singhera, G. K. *et al.* Apoptosis of viral-infected airway epithelial cells limit viral production and is altered by corticosteroid exposure. *Respiratory research* **7**, 78, doi:10.1186/1465-9921-7-78 (2006).
68. Kleinschmidt, M. C., Michaelis, M., Ogbomo, H., Doerr, H.-W. & Cinatl, J. Inhibition of apoptosis prevents West Nile virus induced cell death. *BMC microbiology* **7**, 49–49, doi:10.1186/1471-2180-7-49 (2007).
69. Samuel, M. A., Morrey, J. D. & Diamond, M. S. Caspase 3-dependent cell death of neurons contributes to the pathogenesis of West Nile virus encephalitis. *Journal of virology* **81**, 2614–2623, doi:10.1128/jvi.02311-06 (2007).
70. Barber, G. N. Host defense, viruses and apoptosis. *Cell death and differentiation* **8**, 113–126, doi:10.1038/sj.cdd.4400823 (2001).
71. Labzin, L. I., Lauterbach, M. A. & Latz, E. Interferons and inflammasomes: Cooperation and counterregulation in disease. *The Journal of allergy and clinical immunology* **138**, 37–46, doi:10.1016/j.jaci.2016.05.010 (2016).
72. Rathinam, V. A. K. *et al.* The AIM2 inflammasome is essential for host-defense against cytosolic bacteria and DNA viruses. *Nature immunology* **11**, 395–402, doi:10.1038/ni.1864 (2010).
73. Chen, I. Y. & Ichinohe, T. Response of host inflammasomes to viral infection. *Trends in Microbiology* **23**, 55–63, doi:10.1016/j.tim.2014.09.007.
74. Bauernfeind, F. & Hornung, V. Of inflammasomes and pathogens—sensing of microbes by the inflammasome. *EMBO molecular medicine* **5**, 814–826, doi:10.1002/emmm.201201771 (2013).
75. Wang, H. *et al.* Reciprocal Regulation between Enterovirus 71 and the NLRP3 Inflammasome. *Cell reports* **12**, 42–48, doi:10.1016/j.celrep.2015.05.047 (2015).
76. Ye, N. *et al.* Cytokine responses and correlations thereof with clinical profiles in children with enterovirus 71 infections. *BMC infectious diseases* **15**, 225, doi:10.1186/s12879-015-0965-1 (2015).
77. Wang, S.-M. *et al.* Pathogenesis of Enterovirus 71 Brainstem Encephalitis in Pediatric Patients: Roles of Cytokines and Cellular Immune Activation in Patients with Pulmonary Edema. *Journal of Infectious Diseases* **188**, 564–570 (2003).
78. Lin, T. Y. *et al.* Different proinflammatory reactions in fatal and non-fatal enterovirus 71 infections: implications for early recognition and therapy. *Acta paediatrica (Oslo, Norway: 1992)* **91**, 632–635 (2002).
79. Wang, S. M. *et al.* Acute chemokine response in the blood and cerebrospinal fluid of children with enterovirus 71-associated brainstem encephalitis. *The Journal of infectious diseases* **198**, 1002–1006, doi:10.1086/591462 (2008).
80. Jacobs, S. R. & Damania, B. NLRs, inflammasomes, and viral infection. *Journal of leukocyte biology* **92**, 469–477, doi:10.1189/jlb.0312132 (2012).
81. Mikael Kubista, J. B., David, S. & Robert, S. RNA quality matters. *qPCR* **17**, 63–67 (2012).
82. Beck, S. E. *et al.* Comparison of UV-Induced Inactivation and RNA Damage in MS2 Phage across the Germicidal UV Spectrum. *Applied and environmental microbiology* **82**, 1468–1474 (2016).
83. Rae, C. *et al.* Chemical Addressability of Ultraviolet-Inactivated Viral Nanoparticles (VNPs). *PLOS ONE* **3**, e3315, doi:10.1371/journal.pone.0003315 (2008).
84. Warren, S. E. *et al.* Cutting Edge: Cytosolic Bacterial DNA Activates the Inflammasome via Aim2. *Journal of immunology (Baltimore, Md.: 1950)* **185**, 818–821, doi:10.4049/jimmunol.1000724 (2010).
85. Kärber, G. Beitrag zur kollektiven Behandlung pharmakologischer Reihenversuche. *Archiv f. experiment. Pathol. u. Pharmakol* **162**, 480–483, doi:10.1007/BF01863914 (1931).
86. Arita, M. *et al.* An attenuated strain of enterovirus 71 belonging to genotype a showed a broad spectrum of antigenicity with attenuated neurovirulence in cynomolgus monkeys. *Journal of virology* **81**, 9386–9395, doi:10.1128/jvi.02856-06 (2007).
87. Hufbauer, M. *et al.* Expression of betapapillomavirus oncogenes increases the number of keratinocytes with stem cell-like properties. *Journal of Virology* **87**, 12158–12165, doi:10.1128/jvi.01510-13 (2013).
88. Paterson, A. M. *et al.* The programmed death-1 ligand 1:B7-1 pathway restrains diabetogenic effector T cells *in vivo*. *Journal of Immunology* **187**, 1097–1105, doi:10.4049/jimmunol.1003496 (2011).
89. Turner, J. E. *et al.* IL-9-mediated survival of type 2 innate lymphoid cells promotes damage control in helminth-induced lung inflammation. *The Journal of experimental medicine* **210**, 2951–2965, doi:10.1084/jem.20130071 (2013).
90. Batchelor, R. H., Sarkez, A., Cox, W. G. & Johnson, I. Fluorometric assay for quantitation of biotin covalently attached to proteins and nucleic acids. *Biotechniques* **43**, 503–507 (2007).
91. Kovarova, M. *et al.* NLRP1 dependent pyroptosis leads to acute lung injury and morbidity in mice. *Journal of immunology (Baltimore, Md.: 1950)* **189**, 2006–2016, doi:10.4049/jimmunol.1201065 (2012).
92. Lichlyter, D. J., Grant, S. A. & Soykan, O. Development of a novel FRET immunosensor technique. *Biosensors & bioelectronics* **19**, 219–226 (2003).
93. Nuanalsuwan, S. & Cliver, D. O. Infectivity of RNA from Inactivated Poliovirus. *Applied and environmental microbiology* **69**, 1629–1632 (2003).
94. Zhen, J. *et al.* AIM2 mediates inflammation-associated renal damage in hepatitis B virus-associated glomerulonephritis by regulating caspase-1, IL-1 $\beta$ , and IL-18. *Mediators of inflammation* **2014**, 190860, doi:10.1155/2014/190860 (2014).
95. Wong, K. T. *et al.* The distribution of inflammation and virus in human enterovirus 71 encephalomyelitis suggests possible viral spread by neural pathways. *Journal of neuropathology and experimental neurology* **67**, 162–169, doi:10.1097/nen.0b013e318163a990 (2008).
96. Kämmerer, U. *et al.* A New Rapid Immunohistochemical Staining Technique Using the EnVision Antibody Complex. *Journal of Histochemistry & Cytochemistry* **49**, 623–630 (2001).

## Acknowledgements

This study was supported by the Ministry of Higher Education and High Impact Research Grant (H20001-E00004). We would like to thank Dr. Sangeetha from Medical Biotechnology Lab, Faculty of Medicine, University of Malaya for help on flow cytometry analysis.

## Author Contributions

T.Y., K.C.O., K.T.W. design the experiments and analysed the data. T.Y. performed the experiments and analysed the data. K.C.O., K.T.W. and D.P. provided materials. T.Y., K.C.O. and K.T.W. wrote the paper.

## Additional Information

**Supplementary information** accompanies this paper at doi:10.1038/s41598-017-05589-2

**Competing Interests:** The authors declare that they have no competing interests.

**Publisher's note:** Springer Nature remains neutral with regard to jurisdictional claims in published maps and institutional affiliations.



**Open Access** This article is licensed under a Creative Commons Attribution 4.0 International License, which permits use, sharing, adaptation, distribution and reproduction in any medium or format, as long as you give appropriate credit to the original author(s) and the source, provide a link to the Creative Commons license, and indicate if changes were made. The images or other third party material in this article are included in the article's Creative Commons license, unless indicated otherwise in a credit line to the material. If material is not included in the article's Creative Commons license and your intended use is not permitted by statutory regulation or exceeds the permitted use, you will need to obtain permission directly from the copyright holder. To view a copy of this license, visit <http://creativecommons.org/licenses/by/4.0/>.

© The Author(s) 2017